Ultrahigh-Resolution X-ray Tomography

W. S. Haddad,* I. McNulty, J. E. Trebes, E. H. Anderson, R. A. Levesque, L. Yang

Ultrahigh-resolution three-dimensional images of a microscopic test object were made with soft x-rays collected with a scanning transmission x-ray microscope. The test object consisted of two different patterns of gold bars on silicon nitride windows that were separated by ~5 micrometers. Depth resolution comparable to the transverse resolution was achieved by recording nine two-dimensional images of the object at angles between −50 and +55 degrees with respect to the beam axis. The projections were then combined tomographically to form a three-dimensional image by means of an algebraic reconstruction technique. A transverse resolution of ~1000 angstroms was observed. Artifacts in the reconstruction limited the overall depth resolution to ~6000 angstroms; however, some features were clearly reconstructed with a depth resolution of ~1000 angstroms.

For many years, x-ray microscopy has been an active area of research, but it is now beginning to emerge as a viable imaging tool for microbiologists and materials scientists (*1–3*). X-rays are well suited to three-dimensional (3D) imaging for several reasons. Contrast for specific features in a wide variety of samples can be achieved by exploiting features of the x-ray absorption spectrum. High penetration depths can also be achieved with x-rays; thus, sectioning of the sample can be avoided. Soft x-rays (photon energies near 0.5 keV) are particularly suited to biological microscopy because of their penetration depth. They allow imaging of thick, wet, and initially living microscopic biological specimens, and they cause less radiation damage than electrons for images of equal contrast (*4*). Several groups have developed x-ray microscopes of various types with synchrotron sources (*5*, *6*), laser plasma sources (*7*), and x-ray lasers (*8*). Transverse resolutions well below 0.1 μm have been demonstrated with scanning transmission x-ray microscopes (STXMs) by Jacobsen *et al.* (*5*) and Meyer-Ilse *et al.* (*6*). There are, however, no x-ray optics having sufficiently high numerical aperture (NA) to achieve resolution in depth that is comparable with the transverse resolution. Currently, the best zone plates have a NA < 0.1 for soft x-rays (*9*). The ratio of depth resolution to transverse resolution $\partial_l/\partial_t \approx 2/\mathrm{NA} = 20$ for present state-of-the-art zone plates.

In order to improve the depth resolution, it is necessary to increase the effective NA of the imaging system. This can be done by recording several views of the object over a large angular range. If each of the views is taken with a low-NA optic such that the longitudinal extent of the object is less than the depth resolution of the imaging system, then each view will be a 2D projection of the object. It is then possible to reconstruct a 3D image of the object by combining the set of 2D projections tomographically. The quality of the reconstructed image will depend on the quality of the projection data, the number of projections, and the angular range over which the projections are taken. This method has been demonstrated successfully for high-resolution imaging with 36 Å x-rays by McNulty *et al.* (*10*) using Fourier transform holography to image a single gold bar. In the case of a scanning imaging system, the images are recorded incoherently, and therefore, diffraction is not a factor. The system then becomes effectively a first-generation tomographic imaging system (*11*), that is, one based on diffractionless straight-ray tomography.

We have implemented this approach in conjunction with the STXM at the National Synchrotron Light Source (NSLS) in Brookhaven National Laboratory to make a high-resolution 3D image of an artificial test object. The resulting 3D image shows an improvement of nearly an order of magnitude in resolution with 1/10 to 1/100 the number of projections necessary with existing x-ray tomographic techniques.

We fabricated the test object ourselves because no other suitable sample having well-characterized features was readily available. High-resolution electron beam lithography was used to write two different microscopic patterns of gold bars onto two 1000-Å-thick silicon nitride windows (one pattern per window) supported on 2 mm by 12 mm silicon frames. The lithography was done by "liftoff" and electroplating at IBM Research Center (Yorktown Heights, New York) as part of a cooperative research effort between Lawrence Berkeley Laboratory and IBM. The gold patterns were designed to be simple yet contain a range of features of various sizes, gaps, and angles other than 90°. The two windows were aligned such that the patterns overlapped, and the window frames were cemented together, leaving the patterns separated by a gap of about 5 μm. Thus, the overall dimensions of the 3D test object were about 2 μm by 2 μm by 5 μm (Fig. 1).

When forming images with the STXM, it is necessary to filter out higher order foci of the zone plate. This is done by passing the beam, after it has left the zone plate, through an order-sorting aperture (OSA). To maximize the working distance between the zone plate and the sample, we incorporated the OSA into the test object. The OSA was a 7000 Å thick gold mask with a 10 μm by 15 μm aperture centered over pattern A (Fig. 1). The mask was deposited directly onto the silicon nitride window

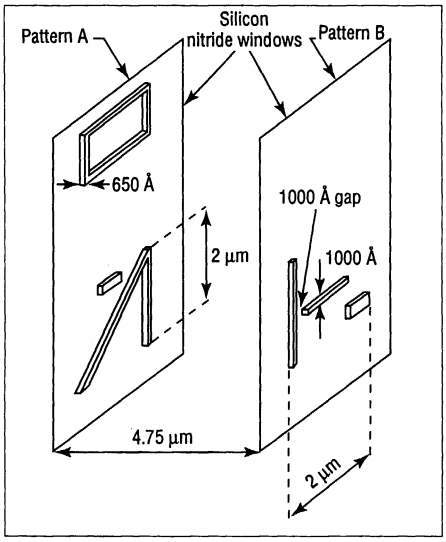

Fig. 1. Sketch of the 3D microscopic test object. The two gold patterns were written by means of electron beam lithography.

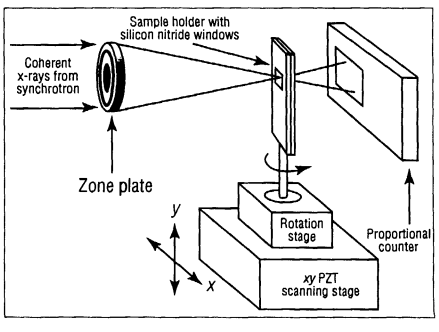

Fig. 2. Sketch of the STXM with the rotatable sample holder added to the PZT piezoelectric translator stage.

W. S. Haddad, J. E. Trebes, R. A. Levesque, University of California, Lawrence Livermore National Laboratory, Livermore, CA 94551, USA.
I. McNulty and L. Yang, Advanced Photon Source, Argonne National Laboratory, Argonne, IL 60439, USA.
E. H. Anderson, Lawrence Berkeley Laboratory, Berkeley, CA 94720, USA.
*To whom correspondence should be addressed.

containing pattern A, and it extended to the edges of the window.

In order to have good contrast while avoiding artifacts in the 3D reconstruction, we carefully chose the thickness of the gold patterns to ensure that the test object would be partially transmissive at the soft x-ray wavelength used to form the images. This means that at points of maximum overall sample thickness, there must be sufficient transmission such that a good signal-to-noise ratio is maintained. In our case, noise is dominated by photon-counting statistics. On the other hand, the bars should be as thick as possible to provide maximum contrast. Computer simulations of the imaging experiment were performed to determine the optimum thickness for the gold bars, and a thickness of 650 Å was consequently chosen for the patterns.

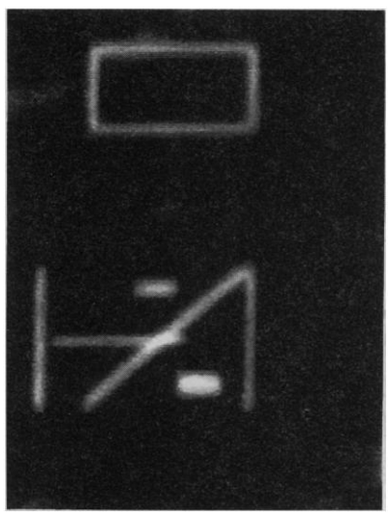

Fig. 3. The normal incidence (0°) projection after processing for alignment, scaling, linearization of the brightness, and correction for various distortions. The negative of the corrected image is shown so that points of high absorption appear bright, whereas points with low absorption appear dark.

The rectangular frame at the top of pattern A was incorporated into the test object as an alignment diagnostic. It has well-defined edges, and its dimensions are precisely known from scanning electron micrographs. This frame was imaged from each viewing angle along with the object and was used as a reference by which to register the individual projections before reconstruction. Because this frame was meant simply as an aid in aligning the projections, the portion of each 2D image containing the frame was not included in the 3D reconstruction.

The 2D projections of the test object were recorded with the use of the STXM on the X1A beamline at the NSLS. The STXM forms images by scanning a sample through a focused beam of x-rays in a raster pattern orthogonal to the beam axis (*5*). We modified the scanning stage of the STXM to include a rotational stage to hold the test object so that the images could be taken over a range of angles (Fig. 2). The x-ray source at X1A is an undulator that produces a high flux of tunable coherent soft x-rays in the energy range of 250 to 800 eV (*12*). For these experiments, the beamline was operated at a wavelength of 36 Å and a spectral width of 0.5%. The x-rays were focused onto the test object by a zone plate with a finest zone width of 600 Å. This produces a near diffraction limited spot with a radius of 1.22 times the finest zone width, about 732 Å (*13*). Scans were made with a step size of 250 Å, which is near the lower limit at which the scanning stage can be operated reliably; therefore, the sampling rate was about 3:1. To have favorable counting statistics, we irradiated the sample with $\sim 10^4$ photons at each point (pixel) of the scan. This required a dwell time of ~10 ms per pixel in each 2D scan. Thus, a typical image containing 250 × 200 pixels took ~500 s to acquire. The total dose delivered to the sample per 2D scan was about 2.2×10^6 Gy (1 Gy = 1 J kg^{-1}). This value is based on an estimate of the total mass of the gold in the test object, the measured incident x-ray flux, and the total transmitted flux in the image. This dose is acceptable for most samples of interest in materials science and microfabrication analysis. It is, however, high for most biological samples. Although high doses will be required for useful high-resolution 3D images, it should not in general be necessary to use levels of irradiation as high

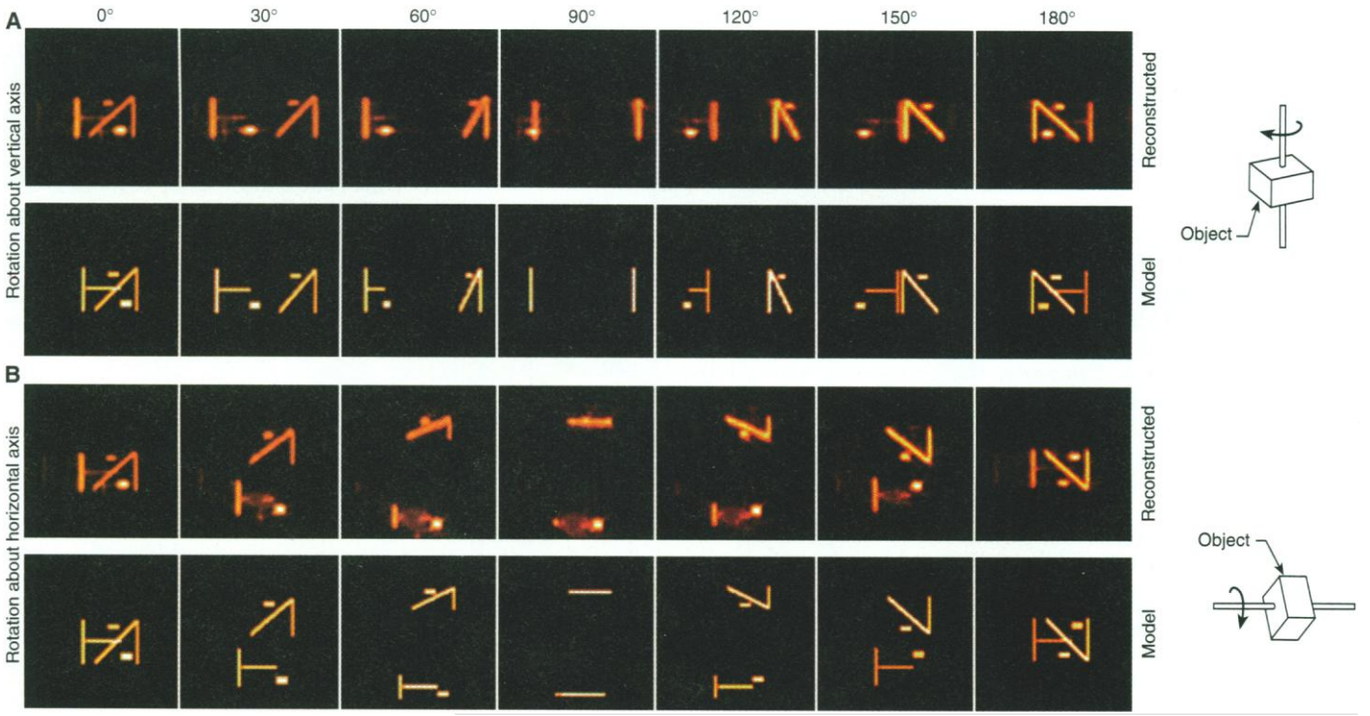

Fig. 4. Views of the 3D reconstruction at various orientations. Each image is a perspective, not a simple projection, of the object with a rotation of 30° between images: (**A**) rotation about a vertical axis and (**B**) rotation about a horizontal axis. The top row of each pair contains images of the actual reconstructed data and the bottom row of each pair shows an ideal scale model of the test object for comparison.

as were used in this experiment. The required dose for 3D image formation is discussed elsewhere (*14*). In addition, it may be possible to use a technique such as cryofixation, which can increase the tolerable dose for biological specimens 100-fold or more (*15*).

Physical limitations of the instrument allowed only a small number of projection images to be taken and restricted the angular range over which projections could be recorded. For this experiment, nine projection images were recorded at angles between −50° and +55°. In this case, the angular limits were forced by occlusion of the extremities of pattern B by the OSA. We recorded nine projections because we felt this was the maximum number that would be practical with the system. The raw projection data were corrected for irregularities before reconstruction was attempted. The two most significant of these were skewing of the images, which resulted from nonorthogonality of the x and y components of the scanning stage, and nonuniformities in the brightness of the projections. The logarithm of the brightness of each projection was also taken before reconstruction to linearize the brightness as a function of material thickness. Figure 3 shows the 0° projection (patterns normal to the beam axis) after processing for alignment, scaling, and correction of distortions.

The combination of limited viewing angle and few projections results in a challenging image reconstruction problem. Neither filtered nor unfiltered back projection methods are satisfactory in this case. Unfiltered back projection does produce recognizable reconstructions of 2D slices for simple objects under these conditions, but the reconstructed slices contain so many artifacts that a 3D reconstruction with this method becomes unintelligible. It is therefore necessary to use an iterative optimization method for reconstruction. We used a computer code based on algebraic reconstruction technique (ART) to form a volumetric data set of the object from the set of 2D projections (*16*, *17*). It has been shown that for limited data tomography problems, ART yields the best results, largely because of its stability when the data contain noise (*17*). Test runs were performed on several 2D slices to determine the optimum number of iterations for the ART code. Only marginal improvement in the image was obtained when the number of iterations was increased from 10 to 15. No noticeable improvements resulted when 30 iterations were used, and some additional small artifacts began to appear. The code was therefore run with 15 iterations per 2D slice. We observed a transverse resolution of ~750 Å in the 2D images. This can be inferred from feature edges and the resolution of the 1000 Å gap in pattern B (Fig. 3). Artifacts in the 3D reconstruction limit the depth resolution while producing a loss in transverse resolution compared with the 2D images. The sources of these artifacts include noise in the 2D projections, uncertainty of ±0.5° in the measurements of the projection angles, misalignment of the projections, the limited angular range over which the projections are recorded, the limited number of projections, and fundamental limits of the reconstruction technique. The most influential of these errors appear to be the inaccuracies in the angular measurements and alignment of the projections. As a result, the transverse resolution in the 3D reconstruction is close to 1000 Å. The overall depth resolution is limited to about 6000 Å, but some features are clearly resolved at 1000 Å in depth.

Figure 4 is a series of 2D-rendered images of the 3D reconstruction along with identical images of an ideal 3D scale model of the test object for comparison. Most noteworthy are the views presented for angles of rotation about the horizontal axis (Fig. 4B) because 2D projections from similar angles were not recorded. Clearly visible are the two patterns shown in Fig. 1. The effects of the reconstruction artifacts can be seen in Fig. 4. The only feature suffering from significant distortion is the horizontal bar of pattern B, which has ballooned to a full width at half maximum of about 6000 Å in the depth dimension. This is a result of the limited angular range over which projections were taken and the inability of the ART algorithm to confine the mass of the feature in the depth direction with the limited data set. Examination of individual slices through the 3D data set shows the vertical bars and the 45° angled bar (pattern A) as bright spots, indicating excellent resolution of these features both transversely and in depth. Despite the loss of transverse resolution after reconstruction, the 1000 Å gap in pattern B is also well resolved. The spacing of the two silicon nitride windows as measured in the reconstructed image is 4.75 μm. This matches the measurement of 5 ± 1 μm made with a high-NA optical microscope. In the 3D image of pattern B, the large 3000 Å by 5000 Å rectangular feature is nearly twice as thick as the long 1000 Å wide bars. This is not a reconstruction artifact, but a real feature in the test object. The thickness anomaly was confirmed by comparison of the x-ray absorption by the rectangle with the absorption by the other features of the test object. Although this thickness anomaly occurred inadvertently in the fabrication process, it provides another indication of the capabilities of the imaging technique presented here.

The 3D reconstructions have depth resolution comparable to the high transverse resolution of the 2D images and, to our knowledge, are the highest resolution x-ray tomographic images to date (*18*, *19*). At present, the resolution is limited by the zone plate; therefore, with today's best zone plates (*9*), resolutions on the order of 300 Å should be attainable. Although higher imaging resolution entails a concomitantly higher dose, radiation-resistant specimens such as sperm cells or techniques such as cryofixation, site-specific gold labeling, or other contrast improving methods may remove the issue of radiation damage. Moreover, ART and related reconstruction algorithms that perform well with limited data sets are likely to reduce the total dose required to record reconstructible x-ray tomograms. This technique should be directly applicable to a wide variety of samples in materials science and biology that are not easily approachable with electrons or other probes.

REFERENCES AND NOTES

1. M. R. Howells, J. Kirz, D. Sayre, *Sci. Am.* **264** (no. 2), 88 (February 1991).
2. For example, see G. Schmahl and D. Rudolph, Eds., *X-Ray Microscopy* (Springer-Verlag, Berlin, 1984); D. Sayre, M. Howells, J. Kirz, H. M. Rarback, Eds., *X-Ray Microscopy II* (Springer-Verlag, Berlin, 1988).
3. Also see A. Michette, G. Morrison, C. Buckley, Eds., *X-Ray Microscopy III* (Springer-Verlag, Berlin, 1991).
4. D. Sayre, J. Kirz, R. Feder, D. M. Kim, E. Spiller, *Science* **196,** 1339 (1977).
5. C. Jacobsen *et al.*, *Opt. Commun.* **86**, 351 (1991).
6. W. Meyer-Ilse *et al.*, in (*3*), pp. 284–289.
7. T. Tomie *et al.*, *Science* **252**, 691 (1991).
8. L. B. Da Silva *et al.*, *ibid.* **258**, 269 (1992).
9. E. H. Anderson and D. Kern, in (*3*), pp. 75–78.
10. I. McNulty *et al.*, *SPIE Proc.* **1741**, 78 (1992).
11. J. C. Russ, *The Image Processing Handbook* (CRC Press, Boca Raton, FL, 1992), p. 364.
12. H. Rarback *et al.*, *J. X-ray Sci. Tech.* **2**, 274 (1990).
13. C. Jacobsen, J. Kirz, S. Williams, *Ultramicroscopy* **47**, 55 (1992).
14. B. E. H. Saxberg and W. O. Saxton, *ibid.* **6**, 85 (1981); R. Hegerl and W. Hoppe, *Z. Naturforsch.* **31**, 1717 (1976); M. van Heel, *Optik* **73** (no. 2), 83 (1986); J. Llacer and M. R. Howells, *Lawrence Berkeley Laboratory Rep. LBL-34000* (1993).
15. J. Dubochet *et al.*, *Q. Rev. Biophys.* **21**, 129 (1988).
16. A. C. Kak and M. Slaney, *Principles of Computerized Tomographic Imaging* (IEEE Press, New York, 1988), chap. 3.
17. D. Verhoeven, *Appl. Opt.* **32**, 3736 (1993).
18. B. P. Flannery, H. W. Deckman, W. G. Roberge, K. L. D'Amico, *Science* **237**, 1439 (1987).
19. J. H. Kinney *et al.*, *ibid.* **260**, 789 (1993).

20. We thank the IBM research staff for their involvement in fabricating the test patterns and the staff at the X1A beamline at NSLS for their support. This work was performed under the auspices of the U.S. Department of Energy (DOE) under contracts W-7405-ENG-48 and W–31–109-ENG-38. The lithography work was supported by the Director, Office of Energy Research, DOE Office of Basic Energy Science, under contract DE–AC03–76SF00098. The NSLS is supported by the DOE Office of Basic Energy Sciences. The X1A beamline is supported by the DOE under grant FG02-89ER60858.

20 May 1994; accepted 20 September 1994